Advances in integrated polarization detectors with innovative features

BU Yong-Hao[1,2], ZHOU Jing[1,2], DENG Jie[1,2], WANG Ruo-Wen[1,2], YE Tao[1,2], SHI Meng-Die[1,2], HUANG Jun-Wei[1,2], ZHANG Yu-Jie[1,2], NING Jun[1,2], LU Wei[1,2], CHEN Xiao-Shuang[1,2]

（1. State Key Laboratory of Infrared Physics, Shanghai Institute of Technical Physics, Chinese Academy of Sciences, Shanghai 200083, China；
2. University of Chinese Academy of Sciences, Beijing 100049, China）

Abstract：The polarization properties of light are widely applied in imaging, communications, materials analysis, and life sciences. Various methods have been developed that can measure the polarization information of a target. However, conventional polarization detection systems are often bulky and complex, limiting their potential for broader applications. To address the challenges of miniaturization, integrated polarization detectors have been extensively explored in recent years, achieving significant advancements in performance and functionality. In this review, we focus mainly on integrated polarization detectors with innovative features, including infinitely high polarization discrimination, ultrahigh sensitivity to polarization state change, full Stokes parameters measurement, and simultaneous perception of polarization and other key properties of light. Lastly, we discuss the opportunities and challenges for the future development of integrated polarization photodetectors.

Key words：integrated polarization detector, infinite polarization extinction ratio, polarization state change detection, full-Stokes, multidimensional detection

具有变革性特征的集成式偏振探测器研究进展

布勇浩[1,2]，周 靖[1,2]，邓 杰[1,2]，王若文[1,2]，叶 韬[1,2]，石梦碟[1,2]，黄俊伟[1,2]，
章雨婕[1,2]，宁 珺[1,2]，陆 卫[1,2]，陈效双[1,2]
（1. 中国科学院上海技术物理研究所 红外科学与技术全国重点实验室，上海 200083；
2. 中国科学院大学，北京 100049）

摘要：光的偏振特性被广泛应用于成像、通信、材料分析和生命科学等领域。已经开发了各种可以用来测量目标偏振信息的方法。然而，传统的偏振探测系统往往体积庞大、结构复杂，限制了其广泛应用的潜力。为了应对微型化的挑战，近年来人们对集成式偏振探测器进行了广泛探索，在性能和功能方面取得了显著进步。在这篇综述中，我们主要关注具有变革性特征的集成式偏振探测器，包括无限高的偏振分辨能力、对偏振态变化的超高灵敏度感知、全斯托克斯参数测量，以及同时感知偏振和光的其他关键特性。最后，我们讨论了集成式偏振光探测器未来发展的机遇和挑战。

关 键 词：集成式偏振探测器；无穷大偏振消光比；偏振态变化探测；全斯托克斯；多维探测

中图分类号：O43　　　　　　　　**文献标识码**：A

Introduction

Light is a type of transverse electromagnetic wave, and polarization is one of its most fundamental properties, which has been widely and deeply applied in many fields, such as imaging[1-4], communication[5-10], material analysis[11], and life sciences[12-15]. Polarized light mainly includes linear polarized light and circular polarized light. Circular polarized light can be further divided into Left-handed Circularly Polarized (LCP) light and Right-handed Circularly Polarized (RCP) light. The Polarization Extinction Ratio (PER) is one of the most critical performance indicators in evaluating polarization detectors or polarization detection systems. The PER is defined as the ratio of the responsivity for the primary detection polarization state to that for the polarization state orthogonal to the primary detection polarization state[16]. This indicator is used to characterize the polarization discrimination ability of the polarization detector. In practical applications, a commonly used method for measuring the polarization information of a target is the Stokes parameter method, which includes four Stokes parameters: S_0, S_1, S_2, and S_3[17-19]. Here, S_0 represents the total intensity of the polarized light, S_1 indicates the difference in components of the polarized light along the $0°$ and $90°$ directions, S_2 represents the difference in components along the $45°$ and $135°$ directions, while S_3 denotes the intensity difference between right-handed circular polarized light and left-handed circular polarized light[20].

Traditional polarization detectors are divided into two categories: 'division of time' and 'division of amplitude'[21]. A division-of-time polarimeter measures the intensities of different polarization states sequentially over time by rotating a waveplate or polarizer, significantly restricting temporal resolution. In contrast, a division-of-amplitude polarimeter separates incident light into distinct photosensitive regions using a sophisticated optical system, leading to a large and complex structure. The demand for real-time polarization imaging and the miniaturization of polarimeters has driven extensive research into the development of integrated polarization detectors[16-17, 22-26]. However, the ultra-compact structure, light diffraction, scattering, and near-field light absorption pose some challenges for the development of integrated polarization detectors: (1) the PERs of integrated polarization detectors are usually 2 to 3 orders of magnitude lower than that of a polarization detection system consisting of discrete polarization optics and a detector; (2) integrated polarization detectors are much less sensitive to changes in polarization state than their traditional counterparts; (3) most integrated polarization detectors can only discriminate a few polarization states, but cannot measure the full Stokes parameters. Furthermore, with the increasing demands for multi-dimensional information perception, integrated polarization detectors are desired to be able to simultaneously perceive other key properties of light along with polarization.

To address the challenges outlined above, researchers have proposed various new theories, methods, and structures, leading to integrated polarization detectors with innovative features and high performance. This review focuses on these innovative advancements, systematically presenting cutting-edge developments in integrated polarization detectors. Topics include integrated polarization detectors with $\infty/-\infty$ PERs, those with ultra-high sensitivity to polarization state changes, those capable of one-shot full Stokes parameter measurement, and those capable of simultaneously sensing polarization along with other key optical properties. The reasons and solutions for these challenges are summarized in Table 1. Finally, the paper discusses future opportunities and challenges in the development of integrated polarization optoelectronic detectors.

Table 1 Challenges in the development of integrated polarization detectors: reasons and solutions

表1 集成式偏振探测器开发过程中的挑战：原因和解决方案

	Challenges	Reasons	New theories, methods, and structures
Part 1	The insufficient PER	Less efficient suppression of the residual photoresponse.	1. Light field−electric field joint manipulation 2. Optoelectronic silent state 3. Band modulation using heterostructures
Part 2	Less sensitive to polarization state changes	Excessive noise in the device	Polarization balanced mode detection
Part 3	1. Only a small number of polarization states can be perceived. 2. Large reconstruction errors in the Stokes parameters	1. Lack of theoretical models to describe the intrinsic correlation between incident optical Stokes vectors and photoresponse. 2. Insufficient accuracy of traditional reconstruction algorithms.	1. Superpixel detectors 2. Optoelectronic polarization eigenvector 3. Use of artificial intelligence algorithms
Part 4	Insufficient perceptible dimensions of light field information	1. Conventional detectors only perceive the intensity information. 2. Multidimensional information reconstruction is difficult.	1. Development of single−pixel detectors capable of perceiving multi−dimensional information. 2. Integrate metasurfaces on commercial cameras 3. Use artificial intelligence algorithms

1　Polarimeter with infinite PER

Conventional polarization detection systems, typically equipped with high-quality polarization optical elements, can achieve linear PERs (LPERs) higher than 10^4. In contrast, the LPERs of integrated polarization detectors are 2 to 3 orders of magnitude lower than that of a polarization detection system consisting of discrete polarization optics and a detector[27-34]. The situation becomes even worse for integrated circular polarization detectors, whose circular polarization extinction ratios (CPERs) are typically lower than five[16]. The insufficient PER of an integrated polarization detector is due to less efficient suppression of the photoresponse to the light in the polarization state orthogonal to the primary detection polarization state, the so-called residual photoresponse[16]. Recently, new effects of polarization photoresponse[23-24, 35-36], novel polarization detection principles[16, 26], and innovative materials and device structures[37-39] have been proposed, leading to $\infty/-\infty$ PER.

To achieve $\infty/-\infty$ PER, the critical factor is to ensure that the residual photoresponse becomes zero. This task is very difficult to achieve by relying solely on the light field manipulation provided by the integrated polarization discriminative structure. The light diffraction, scattering, and near-field absorption at an integrated polarization detector would inevitably generate residual photoresponse. Recent studies reveal that light field-electric field joint manipulation becomes a promising route to achieve this task.

Integration of artificial optical nanoantennas on photosensitive materials is a common method to endow or change their polarization-sensitive properties[17, 25-26, 35, 40-41]. Additionally, artificial optical nanoantennas can effectively enhance the absorption rate of photosensitive materials, thereby improving the photoresponsivity or specific detectivity of photodetectors[16, 26, 40, 42-45]. The in-sensor superposition of nanoantenna induced vectorial non-local photoresponses can achieve zero residual photoresponse and thus $\infty/-\infty$ PER.

In 2021, Wei et al.[23] proposed a mid-infrared semimetal polarization detector with configurable polarity transition and (-1 to $\infty/-\infty$ to 1) PER based on manipulation of vectorial non-local photoresponse (Fig. 1(a)). Both the intensity and direction of the non-local vectorial photocurrent is modulated by the polarization state of the incident light, and the total photocurrent is the superposition of all the vectorial non-local photocurrents. This principle is known as the artificial bulk photovoltaic effect (BPVE). By adjusting the angle of the tapered nanoantenna or choosing different metals to make up the nanoantennas, the PER can be configured to be all possible numbers in the range (-1 to $\infty/-\infty$ to 1).

In 2022, Dai et al.[25] proposed an infrared detector with ultra-high polarization sensitivity (Fig. 1(b)). By leveraging the strong anisotropic absorption of the perfect plasmonic absorber in the infrared region and the localized heating induced by finite-size effects, the detector exhibits polarization-dependent, self-driven photoresponse based on the photothermoelectric effect (PTE).

The operating wavelength is 8 μm. When the polarization direction of the incident light is perpendicular to the resonance direction of the perfect plasmonic absorber, the incident light is reflected. As a result, the Te nanoribbon have no temperature difference throughout the channel, the optical response generated by the PTE is zero, and the PER of the device achieves $\infty/-\infty$.

In 2024, Dai et al.[26] proposed a dynamically reconfigurable polarimetry based on in-sensor differentiation of two self-powered photoresponses with orthogonal polarization dependence and tunable responsivities (Fig. 1(c)). Such a device can be electrostatically configured in an ultrahigh PER mode, where the PER tends to $\infty/-\infty$. Moreover, the device achieves a polarization angle sensitivity of 0.51 mA·W^{-1}·degree^{-1} and a specific polarization angle detectivity of 2.8×10^5 cm·Hz$^{1/2}$·W^{-1}·degree^{-1}. This scheme is demonstrated throughout the near-to-long-wavelength infrared range.

In addition to integrated linear polarization detectors with $\infty/-\infty$ LPERs, integrated linear polarization detectors with $\infty/-\infty$ CPERs have also been invented. In 2023, Bu et al.[16] reported a configurable integrated circular polarization detector based on the optoelectronic silent state, and operating in the NIR region, as shown in Fig. 1(d). By adjusting the ratio of the optical power received by the two chiral plasmonic nanocavities, the total photoresponse of the device is configured to be zero when the incident light is LCP or RCP, thereby the CPER tends to $\infty/-\infty$. Bu et al.[16, 26] proposed the concept of the optoelectronic silent state. In this state, the detector generates not only zero photoresponse but also significantly suppressed noise. The detector can be optoelectronic silent for different polarization states of the incident light, including the randomly polarized state. When the detector is set to be optoelectronic silent for the randomly polarized state of the incident light, a high infrared background is eliminated during the detection and a target in a different polarization state is significantly highlighted compared to the suppressed background.

After inventing these ($\infty/-\infty$)-PER detectors, people realize that the PER is no longer an effective indicator to characterize the polarization discrimination performance of polarization detectors. In this context, Bu et al. define a new PER by taking into account the noise of the detector when the residual photoresponse become zero. As shown in the following equation, the new PER is defined as the ratio of the photoresponse of the detector when illuminated by light in the primary detection polarization state to the noise of the detector when illuminated by light in the polarization state orthogonal to the primary detection polarization state.

$$\mathrm{PER}_{\mathrm{new}} = \frac{I_{\mathrm{ph}}(\mathrm{PDPS})}{I_{\mathrm{noise}}(\perp \mathrm{PDPS})}, \tag{1}$$

where PDPS is the acronym of "primary detection polarization state", and $\perp$PDPS denotes the polarization state orthogonal to the primary detection polarization state. Since the detector in the optoelectronic silent state has a significantly suppressed noise, the PER$_{\mathrm{new}}$ still exceeds the PERs of conventional integrated polarization detec-

tors by more than 4 orders of magnitude（Fig. 1（d））.
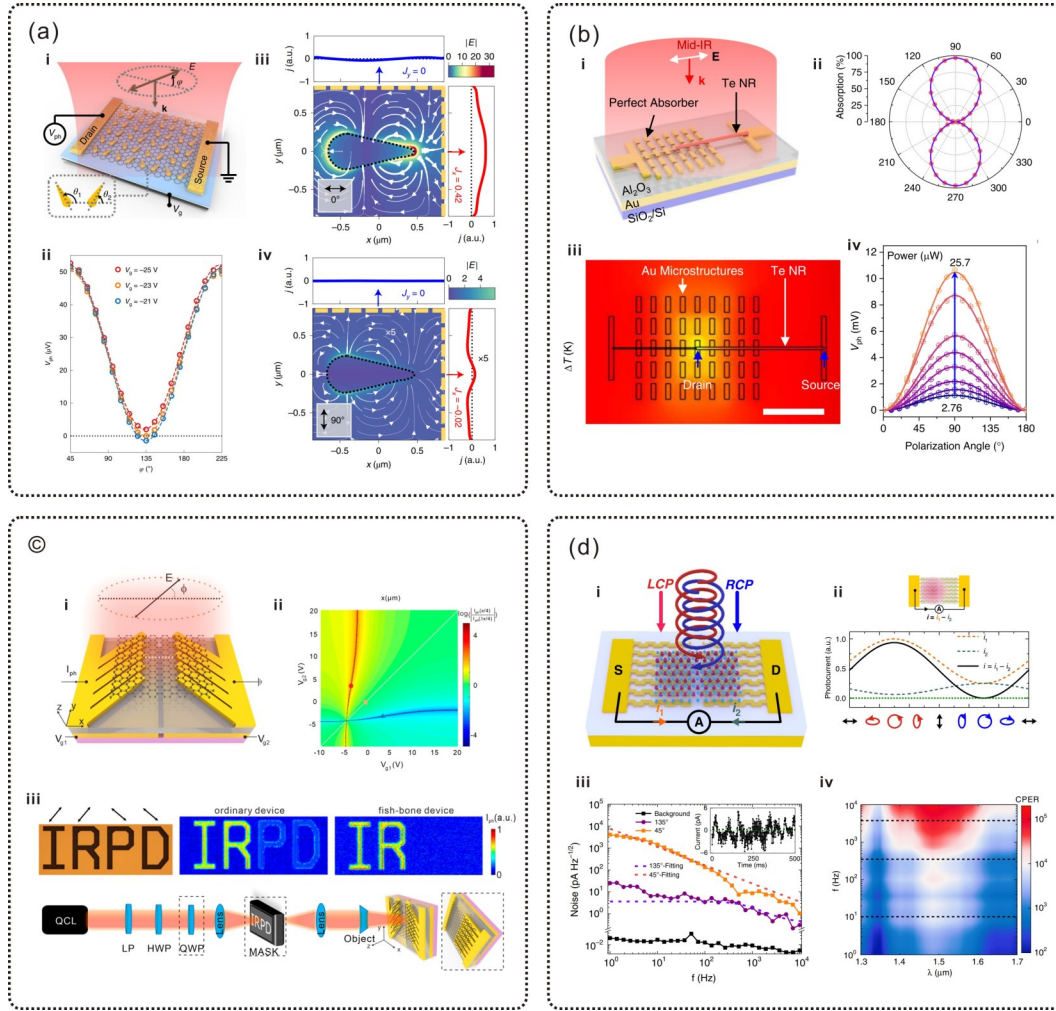
Heterojunctions with special band structures are al-

Fig. 1 （a）Mid-infrared semimetal polarization detector with configurable polarity transition[23]：（i）Schematic of the detector structure and electrical connections；（ii）Polarization-dependent optical response under different gate voltages. When $V_g = -23$ V，the photoresponse induced by 135° polarized light equals 0；（iii）and（iv）Nonlocal vector photocurrent induced by nanoantennas under 0° and 90° polarized light.（b）Te nanoribbon infrared photodetector integrated with a perfect plasmonic absorber on one electrode[25]：（i）Schematic of the device structure；（ii）Polarization-dependent optical absorption characteristics of the perfect plasmonic absorber；（iii）Heating one end of Te using the perfect plasmonic absorber；（iv）Polarization-dependent photoresponse characteristics under different power.（c）Configurable integrated linear polarization detector with a set of orthogonal gratings[32]：（i）Schematic of the device structure；（ii）Modulation of polarization-sensitive characteristics of the detector by adjusting the gate voltage；（iii）Single-pixel imaging.（d）Configurable integrated circular polarization detector based on the optoelectronic silent state[16]：（i）Schematic of the device structure；（ii）Adjustment of the photoresponse of the detector by changing the light spot position，where the photocurrent generated by right-handed circular polarized light can be reduced to 0；（iii）Noise of the device under different polarization angles；（iv）Contour of CPER（wavelength λ，frequency f）of the detector dimer in the LCP-responsive ultrahigh-CPER mode based on experimental data

图1 （a）具有可配置极性转换的中红外半金属偏振探测器[23]：（i）探测器结构和电学连接示意图；（ii）不同栅极电压下的偏振相关光响应。当 $V_g = -23$ V时，135°偏振光诱导的光响应等于0；（iii）和（iv）纳米天线在0°和90°偏振光下诱导的非局域矢量光电流。（b）在一个电极上集成了完美等离子体吸收器的Te纳米带红外光探测器[25]：（i）器件结构示意图；（ii）完美等离子体吸收器的偏振相关光吸收特性；（iii）利用完美等离子体吸收器加热Te的一端；（iv）不同功率下的偏振相关光响应特性。（c）具有一组正交光栅的可配置集式线偏振探测器[32]：（i）器件结构示意图；（ii）通过调节栅极电压调制探测器的偏振敏感特性；（iii）单像素成像。（d）基于光电静默态的可配置集成圆偏振探测器[16]：（i）器件结构示意图；（ii）通过改变光斑位置调节探测器的光响应。其中，右旋圆偏振光产生的光电流可降至0；（iii）不同偏振角下器件的噪声；（iv）在LCP响应-超高CPER模式下基于实验数据计算出的探测器二聚体的CPER（波长 λ、频率 f）等高线

so an effective way to achieve $\infty/-\infty$ PERs. In 2024, Li et al. [37] proposed a polarization photodetector based on the $CdSb_2Se_3Br_2/WSe_2$ heterojunction (Fig. 2(a)). In the $CdSb_2Se_3Br_2/WSe_2$ heterostructure, gate voltage variations control the anisotropic band alignment. This leads to a polarization-dependent shift in the photo-induced threshold voltage (V_{th}), caused by the anisotropic carrier transition. The significant V_{th} shift reverses the polarization photovoltaic current, allowing the PER to switch from positive (unipolar regime) to negative (bipolar regime), covering the entire range of values ($1 \rightarrow \infty/-\infty \rightarrow -1$).

In the same year, Wang et al. [38] discovered a polarization- and gate-tunable optoelectronic reverse in 2D semimetal/semiconductor photovoltaic heterostructure (Fig. 2(b)). By adjusting the gate voltage, the Fermi level in ambipolar WSe_2 can be tuned between the conduction band (CB) and valence band (VB). This enables easy control and inversion of the built-in electric field, resulting in sign reversal of polarization-sensitive photocurrent. With the in-plane anisotropic structure of $1T'$-$MoTe_2$, the device demonstrates highly efficient polarimetric detection, achieving a PER value of up to $\infty/-\infty$.

Combining ferroelectric materials with 2D vdW materials can significantly enhance the performance of polarization detectors[39, 46]. In 2024, Wu et al. [39] proposed a polarization photodetector based on black phosphorus. As shown in Fig. 2(c), the authors found that "T"-shaped ferroelectric domain array broke the intrinsic C_{3v} symmetry of $MoTe_2$ and induced an asymmetric carrier distribution in $MoTe_2$. By applying different bias voltages, the photoresponse corresponding to different polariza-

tion states can be eliminated (Fig. 2(c)(ii)), leading to $\infty/-\infty$ PER.

2　Ultrahigh sensitivity to polarization state changes

Noise-equivalent polarization angle difference ($NE\Delta\chi$, unit：$degree \cdot Hz^{-1/2}$) is a parameter used to assess the sensitivity of a polarization detector to changes in the polarization state of the incident light. It is related to noise (I_{noise}, unit：$A\ Hz^{-1/2}$) and polarization-angle sensitivity (PAS, unit：$A\ degree^{-1}$). The calculation formula is：

$$NE\Delta\chi = \frac{I_{noise}}{PAS} = \frac{A \cdot Hz^{-1/2}}{A \cdot degree^{-1}} = degree \cdot Hz^{-1/2}. \quad (2)$$

$NE\Delta\chi$ refers to the minimum fluctuation in the photoresponse caused by changes in the incident light's polarization state that the polarization detector can resolve. The lower the value, the stronger the capability of the device to sense changes in the polarization state[23].

For ordinary polarization photodetectors, due to their extinction ratio is not high enough to achieve complete shielding of the photocurrent, there is always a current flowing in the device. As a result, the device is often accompanied by substantial noise, such as $1/f$ noise, shot noise, thermal noise, etc[16, 26]. Excessive noise reduces the noise-equivalent polarization-angle rotation performance of the device. In contrast, for polarization detectors with infinite PER, their photocurrent minima can be reduced to zero, and the optoelectronic silent state helps maintain noise at a low level. However, at this point, the polarization-angle sensitivity of the device tends to be zero, and so the noise-equivalent polarization-
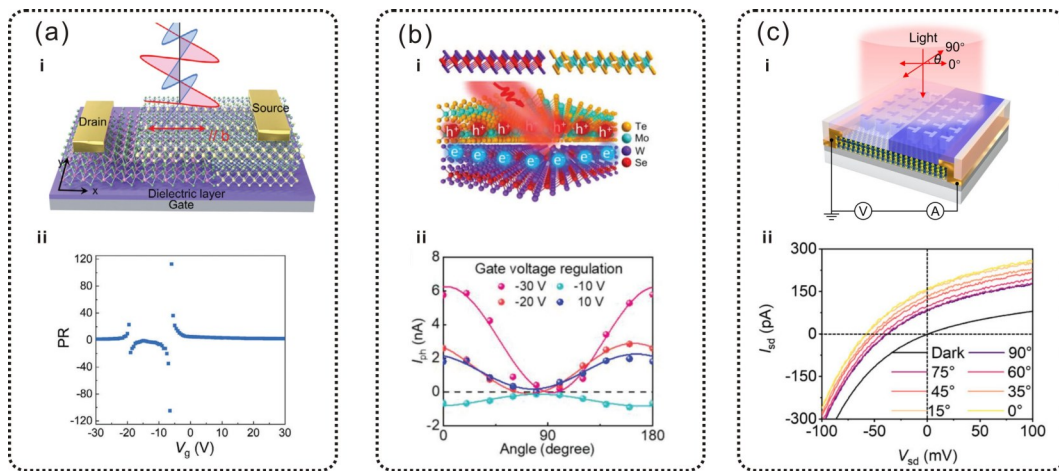

Fig. 2　(a) The polarization photodetector based on $CdSb_2Se_3Br_2/WSe_2$ heterojunction[37]：(i) schematic of the detector structure；(ii) achieving an infinite PER near gate voltages of -20 V and -6 V. (b) photovoltaic heterostructure based on $1T'$-$MoTe_2$ and WSe_2[38]：(i) schematic of the detector materials；(ii) Polarization-dependent photocurrent under different gate voltages. (c) black phosphorus photodetector with BPVE defined by ferroelectric domains[39]：(i) schematic of the detector structure and polarization pattern of the ferroelectric domains；(ii) dependence of the photocurrent on bias voltage under different polarization angles

图2　(a) 基于$CdSb_2Se_3Br_2/WSe_2$异质结的偏振光电探测器[37]：(i) 探测器结构示意图；(ii) 在栅极电压为-20 V和-6 V附近实现无限PER。(b) 基于$1T'$-$MoTe_2$和WSe_2的光伏异质结[38]：(i) 探测器材料示意图；(ii) 不同栅极电压下随偏振变化的光电流。(c) 由铁电畴定义的BPVE黑磷光电探测器[39]：(i) 探测器结构和铁电畴极化模式示意图；(ii) 不同偏振角下光电流对偏置电压的依赖性。

angle reaches infinity, which prevents the detector from sensing small changes in the polarization angle of the incident light. As a result, the minima of noise-equivalent polarization-angle rotation tends to occur in polarization-dependent balanced detectors, which are characterized by a PER equal to −1[24, 35]. In this type of polarization detector, at the point of photocurrent polarity reversal, the polarization-angle sensitivity reaches maximum while the noise intensity remains at the lowest level.

In 2020, Wei et al.[35] proposed a zero-bias mid-infrared graphene photodetector with bulk photoresponse and calibration-free polarization detection, which exhibits cascaded polarization-sensitive photoresponse under uniform illumination, simulating the BPVE. The device's responsivity is three orders of magnitude higher than that of photodetectors based on traditional bulk photovoltaic effects, with a noise-equivalent power of 0.12 nW Hz$^{-1/2}$. As shown in Fig. 3(a), the authors fabricated a metal nanoantenna device with threefold rotation symmetry. The responsivities of the three sets of detection units are the same, with a phase difference of 60° between each set, and the PER of each set of devices is −1.

Ordinary circularly polarization detectors with integrated chiral nanostructures often fail to avoid the response caused by linear polarized light. To address this issue, in 2022, Wei et al.[24] proposed a geometric filterless photodetectors for mid-infrared spin light. As shown in Fig. 3(b), the polarization-dependent photocurrent

demonstrates that the detector is also a circular polarization-balanced detector, capable of blocking responses to S_1 and S_2 parameters. A self-powered optical response rate of 392 V W^{-1}. At a small incident power of 1.8 μW, an optical ellipticity detectivity as low as 0.03 degree Hz$^{-1/2}$ at room temperature.

In 2023, Xie et al.[47] proposed a zero-bias long-wave infrared nanoantenna-mediated graphene photodetector for polarimetric and spectroscopic sensing (Fig. 3(c)). The PER of the detector is −1. By adjusting the near-field distribution of the nanoantenna, the absorption rate of the detector was improved. The noise-equivalent polarization-angle rotation of approximately 0.05° Hz$^{-1/2}$ at the power of 26.6 μW. In addition to the use of metals to fabricate nanoantennas, the idea of preparing polarization detectors by directly processing photosensitive materials has also gained much attention in recent years. In 2024, Zhang et al.[36] reported a high-discrimination, broadband circular polarization photodetector using dielectric achiral nanostructures. As shown in Fig. 3(d), the authors directly etched achiral nanostructures on Te nanosheets. The noise equivalent light ellipticity difference reaches a minimum of 0.03° Hz$^{-1/2}$ at the cut-off frequency.

In addition to the artificial BPVE, polarization-dependent balanced detection can also be achieved using a pair of orthogonal or chiral light-coupling structures[44, 48-49]. In 2015, Lu et al.[48] proposed a thermopile

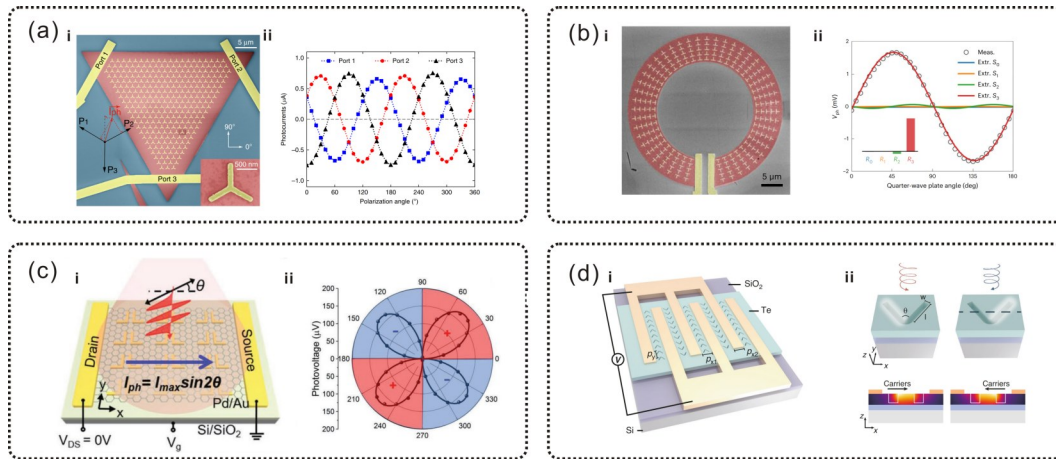

Fig. 3 (a) Zero-bias mid-infrared graphene photodetector with bulk photoresponse and calibration-free polarization detection[35]: (i) schematic diagram of the device structure and electrical connections; (ii) polarization-dependent photocurrent measured at the three ports of the device, all showing a polarization extinction ratio of −1. (b) geometric filterless photodetector[24]: (i) illustration of the T-antenna integrated on graphene; (ii) photocurrent response of the device to different Stokes parameters. (c) zero-bias long-wave infrared nanoantenna-mediated graphene photodetector[47]: (i) schematic representation of the device structure; (ii) bipolar photocurrent response dependent on polarization. (d) circularly polarized light photodetector using dielectric achiral nanostructures[36]: (i) schematic diagram of the device structure; (ii) coupling differences of dielectric achiral nanostructures on left- and right-handed circularly polarized light

图3 （a）具有体光伏响应和免校准偏振探测功能的零偏置中红外石墨烯光电探测器[35]:(i)器件结构和电学连接示意图;(ii)在器件的三个端口测量到的偏振相关光电流,偏振消光比均为−1。(b)几何无滤波器光电探测器[24]:(i)集成在石墨烯上的T型天线示意图;(ii)器件对不同斯托克斯参数的光电流响应。(c)零偏压长波红外纳米天线介导的石墨烯光电探测器[47]:(i)器件结构示意图;(ii)偏振依赖的双极性光电流响应。(d)使用电介质非手性纳米结构的圆偏振光电探测器[36]:(i)器件结构示意图;(ii)电介质非手性纳米结构对左旋和右旋圆偏振光的耦合差异

detector of the light ellipticity (Fig. 4(a)). By constructing a square array, the photoresponses generated by the Stokes parameters S_1 and S_2 are canceled out, enabling the detector to directly output a bipolar photovoltage proportional to the Stokes parameter S_3.

In 2019, Peng et al. [44] proposed a chiral graphene-based mid-infrared photodetector. As shown in Fig. 4 (b), the device integrates nanoantennas with opposite chirality on source and drain electrodes. Surface plasmon resonance enhances the absorption rate of graphene by 17 times, and the device exhibits equal but opposite photoresponses to left- and right-handed circular polarized light. In the same year, Thomaschewski et al. [49] reported a study on circularly polarized light detection using plasmonic nanocircuits. As shown in Fig. 4(c), the authors utilized plasmonic achiral nanocouplers to separate left- and right-handed circularly polarized light and couple them into two plasmonic waveguides. The photocurrents generated by two germanium (Ge) detectors were then processed externally using differential calculations, achieving high-precision resolution of circularly polarized light.

3   On-chip full-Stokes polarimeter

The demand for real-time full Stokes polarimetric imaging has attracted a lot of research interest. To ad-dress this demand, researchers have tried to combine multiple independently polarization detection pixels into a superpixel[50-53] and reconstruct the Stokes parameters of the incident light based on the photoresponses of the sub-pixels and a specific algorithm. This method would reduce the imaging resolution of the detector since many of the pixels originally used for imaging are used to probe the polarization state. Thus, the main challenge lies in designing the polarization dependent optoelectronic properties of the individual pixels to achieve the most accurate acquisition of full Stokes parameters while minimizing the number of the pixels.

For the fabrication of superpixel detectors, integrating different polarization-sensitive structures in different regions of one detection material is a convenient and common approach. In 2020, Li et al. [18] reported the monolithic full-stokes near-infrared polarimetry with a chiral plasmonic metasurface integrated graphene-silicon photodetector. The working wavelength is 1 550 nm. As shown in Fig. 5(a), the same metasurface, arranged in different orientations and handedness, is integrated with each of the four pixels. The four pixels share a common ground terminal, i. e. the Si substrate. Based on the photocurrent values of the four pixels and an empirical algorithm, the full Stokes parameters are reconstructed in one shot. However, the root
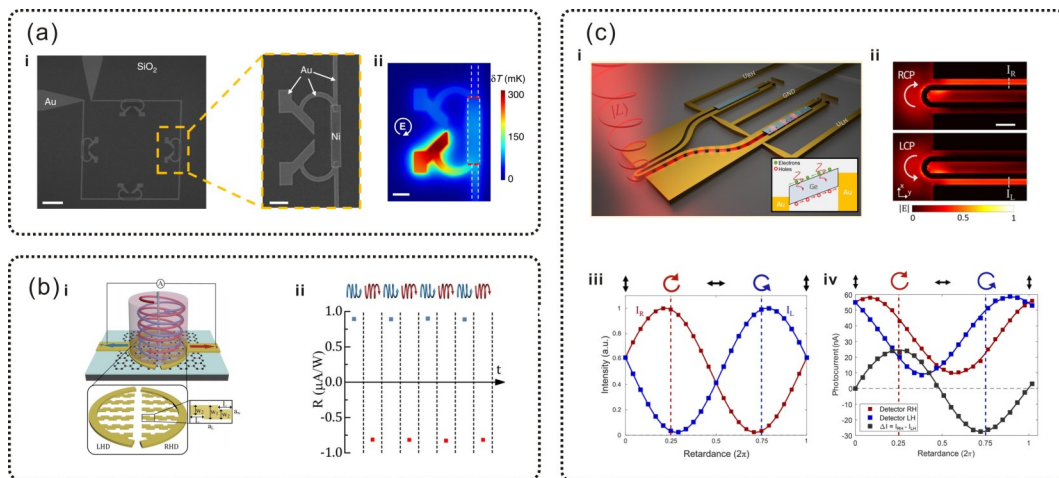

Fig. 4 (a) Thermopile detector capable of measuring optical ellipticity[48]: (i) The unit structure of the device and the spatial distribution of the unit structure; (ii) The patterned Au couples with specific handedness of circularly polarized light, resulting in localized temperature enhancement. (b) A chiral graphene mid-infrared optoelectronic detector[44]: (i) Schematic diagram of the device structure and electrical connections; (ii) The device exhibits photoresponses of equal intensity but opposite direction for left- and right-handed circular polarized light. (c) Plasmonic nanocircuits capable of circularly polarized photodetection[49]: (i) schematic of the structure of the device and the energy band structure of the Ge detector; (ii) Electric field distribution of the device under illumination with different handedness of circular polarized light; (iii) Output intensities of the two channels at different polarization states; and (iv) polarization-differential photocurrents

图 4 (a) 能够测量光学椭圆度的热电堆探测器[48]: (i) 器件的单元结构和单元结构的空间分布; (ii) 图案化 Au 与特定手性的圆偏振光耦合,导致局部温度增强。(b) 手性石墨烯中红外光电探测器[44]: (i) 器件结构和电学连接示意图; (ii) 器件对左手和右手圆偏振光表现出强度相同但方向相反的光响应。(c) 能够进行圆偏振光电探测的等离激元纳米电路[49]: (i) 器件结构示意图和 Ge 探测器的能带结构; (ii) 器件在不同偏振方向的圆偏振光照射下的电场分布; (iii) 两个通道在不同偏振状态下的输出强度; (iv) 偏振差分光电流

mean square errors（RMSEs）of the reconstructed S_1, S_2 and S_3, which are 13%, 17% and 17%, respectively, are not sufficiently low for practical applications. In 2022, Dai et al. [41] proposed an on-chip mid-infrared photothermoelectric detector with $PdSe_2$ as the channel material. As shown in Fig. 5（b）, the device integrates four metasurfaces with different polarization dependent optoelectronic properties. In the experiment, the average measurement errors for Stokes parameters S_1, S_2, and S_3 were 14.2%, 15.2%, and 5.4%, respectively.

In order to enhance the accuracy of full Stokes parameters detection, a proper formalism describing the polarization-dependent photoresponses of metasurface-integrated photodetectors is required. In 2024, Deng et al. [17] proposed the concept of an optoelectronic polarization eigenvector（OPEV）The OPEV, which is a 1×4 vector, expresses the linear relationship between the incident Stokes vector and the photocurrent of a detector. As shown in Fig. 5（c）, each subpixel contains an *in-situ* integrated plasmonic metasurface and corresponds to a distinct OPEV. Combined with a machine learning algorithm, this polarimeter achieves full Stokes parameters reconstruction over the entire polar-ization state range at any light intensity, with a root mean square error less than 1% for each Stokes parameter.

Using only anisotropic or chiral materials to form full-Stokes polarimeters is an effective way to further simplify the device structure（Fig. 5（d））. In 2021, Chen et al. [19] proposed a self-powered, filterless on-chip full Stokes polarimeter based on a monolayer MoS_2/few-layer MoS_2 homojunction. This design allows a full-Stokes polarimeter without an additional filter layer. The RMSEs of the reconstructed Stokes parameters S_1, S_2, and S_3 are >5%, >4.8%, and >6.7%, respectively. It should be noted that this device is not a one-shot polarimeter, and it needs to be rotated around the center axis of the sample holder during operation. In the same year, Ma et al. [54] reported a full-Stokes polarimeter based on chiral Perovskite single crystal（（S- and R-MBA）$_2PbI_4$, where MBA = $C_6H_5C_2H_4NH_3$）. It is important to note that, in order to detect all the linear polarization parameters（S_1 and S_2）, the incident light's tilt angle needs to be continuously adjusted during testing. The average error of the reconstructed Stokes parameters from this detector ranges from 7.5% to 26%.
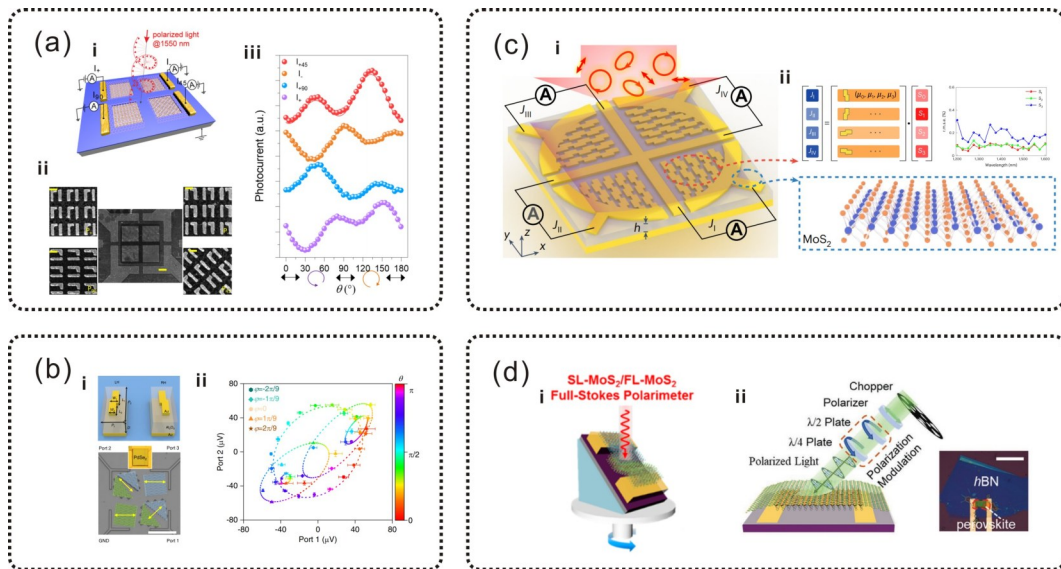

Fig. 5 （a）Graphene-Si full-Stokes detector integrated with chiral plasmonic metasurfaces[18]：（i）schematic of the device structure and electrical connections；（ii）scanning Electron Microscopy（SEM）image of the device；（iii）polarization-dependent characteristics of the photocurrents generated by the four sub-pixels.（b）mid-infrared full-Stokes polarimeter based on PTE[41]：（i）structural parameters of the metasurfaces and optical image；（ii）Two-dimensional plot of Port 1 and Port 2 under different azimuthal angle θ and ellipticity angle φ；（c）on-chip full-Stokes polarimeter based on optoelectronic polarization eigenvectors[17]：（i）schematic of the device structure and electrical connections；（ii）the optoelectronic conversion matrix and the r. m. s. e. values of the Stokes vector components at different wavelengths.（d）full-Stokes polarimeter using only 2D materials, and their incident light needs to be tilted：（i）full-Stokes polarimeter based on SL-MoS$_2$/FL-MoS$_2$ heterostructure[19]；（ii）full-Stokes polarimeter based on chiral perovskites[54]

图5 （a）集成了手性等离激元超表面的石墨烯-硅全斯托克斯探测器[18]：（i）器件结构和电学连接示意图；（ii）器件的扫描电子显微镜（SEM）图像；（iii）四个子像素产生的光电流的偏振依赖特性。（b）基于PTE的中红外全斯托克斯偏振计[41]：（i）超表面的结构参数和光学图像；（ii）端口1和端口2在不同方位角θ和椭圆度角φ下的二维图。（c）基于光电偏振特征矢量的片上全斯托克斯偏振计[17]：（i）器件结构和电学连接示意图；（ii）光电转换矩阵和r. m. s. e. 值。（d）仅使用二维材料的全斯托克斯偏振计，其入射光需要倾斜：（i）基于SL-MoS$_2$/FL-MoS$_2$异质结的全斯托克斯偏振计[19]；（ii）基于手性钙钛矿的全斯托克斯偏振计[54]

4 Increasing the perceptible information dimensions of the polarimeters

Polarization detectors are primarily used to sense the polarization state of light, often overlooking other fundamental properties of light such as wavelength and phase. Expanding the information dimension that polarization detectors can perceive is an important development direction.

4.1 Multidimensional detection enabled by a single-pixel detector

In 2022, Ma et al. [55] first observed the bulk photovoltaic effect in twisted double bilayer graphene (TDBG), which is induced by the moiré-induced strong symmetry breaking and quantum geometric contribution. With the help of artificial neural networks, the authors analyzed and reconstructed the photocurrent, achieving simultaneous detection of the wavelength, polarization, and power of light (Fig. 6(a)).

In 2024, Jiang et al. [56] proposed a broadband multidimensional optoelectronic detector based on metasurfaces. As shown in Fig. 6(b), the authors designed a three-port device with differently structured metasurfaces integrated into the graphene photodetector at each port. By combining machine learning and the Adam optimization algorithm, the detector successfully achieved the resolu-

tion of circularly polarized light in the wavelength range of 1-8 μm. In the same year, Wang et al. [57] used two twisted black arsenic – phosphorus (b-AsP) homojunction to achieve polarization and wavelength detection (Fig. 6(c)). The responsivity of the device is influenced by both wavelength and polarization state. The authors demonstrated simultaneous detection of both polarization and wavelength by plotting the dependence of responsivity on wavelength and polarization state. Zhang et al. [58] developed a multidimensional optical information acquisition device based on a misaligned unipolar barrier photodetector, consisting of a b-AsP/MoS$_2$/BP stacked structure (Fig. 6(d)). The b-AsP/MoS$_2$ and BP/MoS$_2$ heterojunctions can be adjusted by a bias voltage, enabling the sensing of both polarization and spectral information.

4.2 Metasurface integrated polarimetric cameras

Integrating metasurfaces with commercial cameras combines the focal plane array technology with the advanced optical properties of metasurfaces, providing a new solution for high-precision detection of multidimensional optical information.

In 2022, Fan et al. [59] introduced an innovative nanophotonic light-field camera inspired by the optical structure of Trilobite eyes (Fig. 7(a)). This camera incorporates a spin-multiplexed bifocal metalens array, ca-
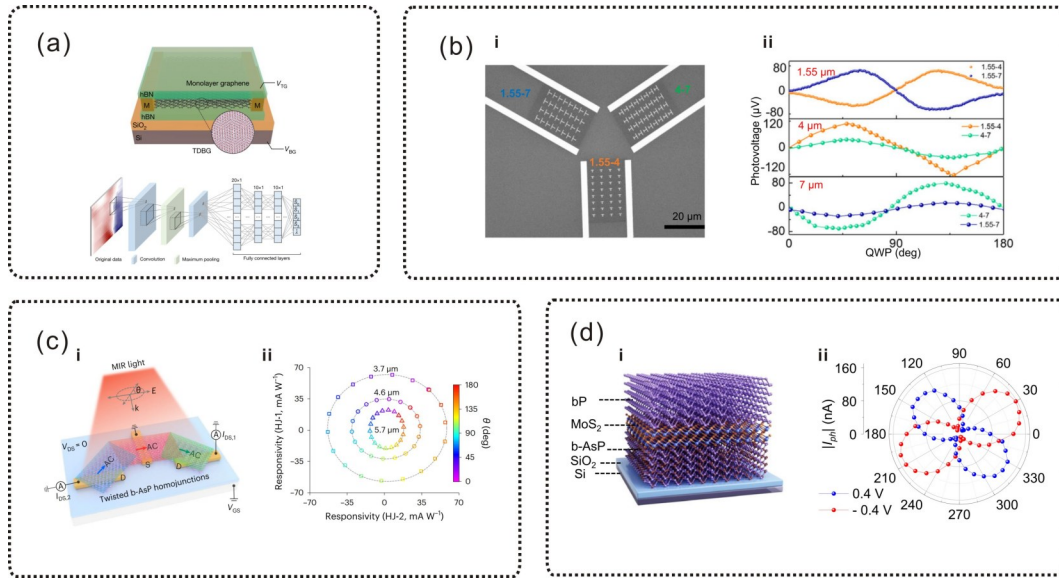

Fig. 6 (a) Structure diagram of a multidimensional optoelectronic detector based on a TDBG and a diagram of an artificial neural network[55]. (b) broadband multidimensional optoelectronic detector based on metasurfaces[56]：(i) SEM image of the detector, with three ports integrated with metasurfaces of different structures；(ii) polarization-dependent photocurrent at wavelengths of 1.55 μm, 4 μm, and 7 μm at the three ports. (c) multidimensional optoelectronic detector based on twisted b-AsP heterojunctions[57]：(i) structural diagram of the detector and electrical connection diagram；(ii) polarization- and wavelength-dependent responsivity at the two ports of the detector. (d) misaligned unipolar barrier photodetector[58]：(i) structure diagram of the detector；(ii) polarization-dependent photocurrent under bias voltages of 0.4 V and −0.4 V

图6 （a）基于 TDBG 的多维光电探测器结构图和人工神经网络图[55]。（b）基于超表面的宽带多维光电探测器[56]：(i) 探测器的扫描电镜图像，三个端口集成了不同结构的超表面；(ii) 三个端口在波长为 1.55 μm、4 μm 和 7 μm 时的偏振相关光电流。（c）基于转角 b-AsP 异质结的多维光电探测器[57]：(i) 探测器的结构图和电学连接图；(ii) 探测器两个端口的偏振和波长共同调制的响应率。（d）错位单极势垒光探测器[58]：(i) 探测器的结构图；(ii) 偏置电压为 0.4 V 和 −0.4 V 时随偏振变化的光电流

pable of capturing high-resolution light-field images with an unprecedented depth-of-field range, spanning from centimeters to kilometers. The metalens array operates efficiently across a wide wavelength range from 460 nm to 700 nm, achieving broadband photonic spin-multiplexing in the visible spectrum.

In 2023, Zuo et al. [50] introduced a chip-integrated metasurface-based Full Stokes Polarimetric Imaging sensor (MetaPolarIm), which combines an ultrathin (~600 nm) Metasurface Polarization Filter array (MPFA) with a visible imaging sensor (Fig. 7(b)). This sensor was fabricated using CMOS-compatible processes, making it highly scalable for mass production. The MPFA features a hybrid dielectric-metal chiral metasurface design along with double-layer nanograting polarizers, providing high polarization sensitivity and accuracy. In practical experiments, the MetaPolarIm sensor achieved measurement errors of less than 2% for all Stokes parameters in red and green colors under normal incidence.

In 2024, Fan et al. [60] proposed an innovative concept that leverages spatial and frequency dispersion at optical interfaces to control polarization and spectral responses in the wavevector domain, combined with deep learning methods to decode polarization and spectral information. They introduced a dispersion-assisted multidimensional detector that enables the detection of high-dimensional optical field information in a single measurement using a single device (Fig. 7(c)). This system does not rely on complex designs or fabricated metasurfaces, yet its performance matches or even exceeds that of advanced commercial polarimeters or spectrometers. This research paves the way for the practical application of high-dimensional optoelectronic detectors.

5 Discussion and outlook

Integrated polarization detectors have achieved notable progress, offering significant benefits in applications like improving image contrast and providing additional information about targets. However, their development encounters several challenges. For detectors integrated with photonic structures, the reliance on resonance restricts their operational wavelength range. Similarly, polarization detectors based on heterojunctions face limited material choices and persistent inaccuracies in Stokes pa-
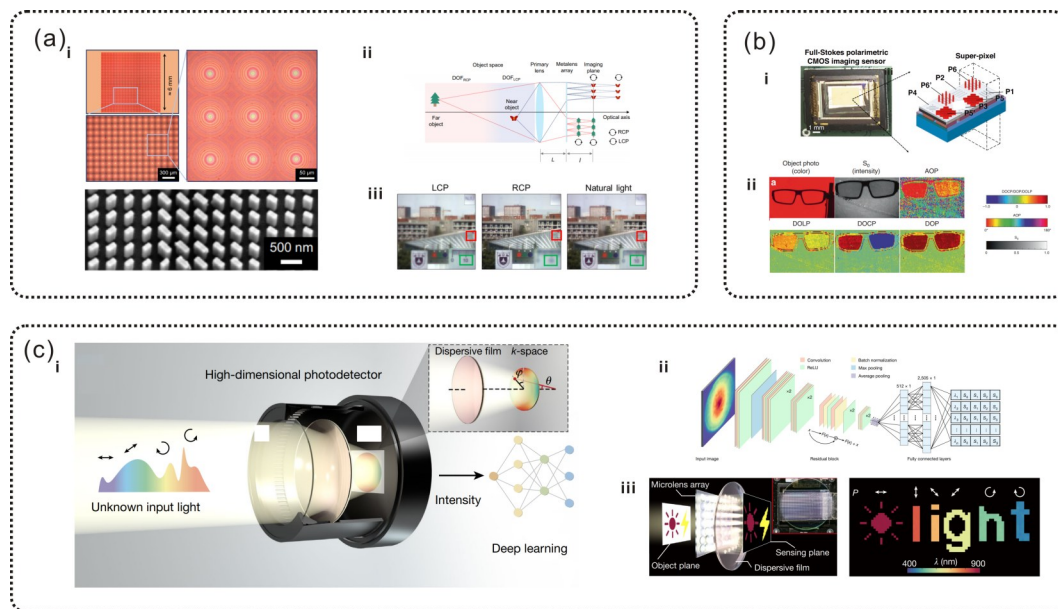

Fig. 7 (a) Trilobite-inspired neural nanophotonic light-field camera with extreme depth-of-field[59]: (ⅰ) Optical microscope image and SEM image of the bioinspired photonic spin-multiplexed metalens array. (ⅱ) Conceptual sketch of the light-field imaging camera and the working principle of the system with metalens array achieving spin-dependent bifocal light-field imaging. (ⅲ) The rendered center-of-view images for LCP, RCP, and natural light. (b) Chip-integrated metasurface full-Stokes polarimetric imaging sensor[50]: (ⅰ) Image of the full Stokes polarimetric CMOS imaging sensor. (ⅱ) A full Stokes polarization image of 3D glasses against an unpolarized background. (c) Dispersion-assisted multidimensional photodetector[60]: (ⅰ) Simultaneous mapping of polarization and spectral information in single-shot imaging; (ⅱ) Schematic of the deep residual network; (ⅲ) Detection of targets with multiple polarization and wavelength information using the multidimensional spectral polarization imager

图7 (a)受三叶虫启发的具有极深景深的神经纳米光子光场相机[59]:(ⅰ)仿生光子自旋多路复用超透镜阵列的光学显微镜图像和SEM图像;(ⅱ)光场成像相机的概念草图和超透镜阵列实现自旋依赖性双焦点光场成像的系统的工作原理;(ⅲ)针对LCP、RCP和自然光渲染的视图中心图像。(b)芯片集成超表面全斯托克斯偏振成像传感器[50]:(ⅰ)全斯托克斯偏振CMOS成像传感器图像;(ⅱ)非偏振背景下3D眼镜的完整斯托克斯偏振图像。(c)色散辅助多维光电探测器[60]:(ⅰ)在单次成像中同时映射偏振和光谱信息;(ⅱ)深度残差网络示意图;(ⅲ)利用多维光谱偏振成像仪检测具有多种偏振和波长信息的目标

rameter reconstruction.

The emergence of polarization detectors with innovative features has addressed several challenges across different fields. In Table 2, we compare representative high-performance integrated polarization detectors with commercial counterparts. The results indicate that in certain application scenarios, these high-performance integrated detectors can outperform commercial devices, demonstrating significant application potential. In terms of response speed, the graphene-based polarization detector utilizing the artificial bulk photovoltaic effect is at least as fast as commercial polarimeters and can theoretically achieve an ultra-fast mid-infrared response of 500 GHz. Its optical responsivity of 27 V W^{-1} surpasses that of some high-speed commercial photodetectors（e. g., the Thorlabs DXM20AF 20 GHz photodetector，which has a responsivity of 0. 9 A W^{-1}）. Meanwhile, the MoS$_2$ polarimeter, based on optoelectronic polarization eigenvectors, achieves a Stokes parameter reconstruction accuracy of less than 1%, whereas the polarization accuracy of commercial polarimeters is typically around 1%（e. g., PAX1000, Thorlabs）.

In the infrared range, a major limitation of reported polarization detectors with PER values of $\infty/-\infty$ or -1 is the lack of characterization using blackbody sources；instead, characterizations are typically conducted with high-performance lasers to assess optoelectronic properties. While lasers allow precise control over light source attributes（such as wavelength, power, spot size, and high-frequency modulation）in a laboratory setting, the resulting performance metrics are primarily suited for applications like spectral measurement, optical communication, or lidar. However, in imaging applications, the main challenge is detecting broad-spectrum, low-energy infrared radiation. The ability to respond to blackbody radiation is a key indicator of an infrared detector's practi-

cal application potential，and thus future research efforts should continue in this direction.

Future advancements in device fabrication could involve novel large-area，narrow-linewidth patterning techniques，such as deep ultraviolet lithography and nanoimprint technology，which could enhance the efficiency of metasurface integration on detectors. On the data processing side, the emergence of more sophisticated artificial intelligence algorithms holds promise for improving the efficiency of multi-Stokes parameter reconstruction and high-dimensional optical information processing. These advancements could significantly reduce computation time and improve reconstruction accuracy，paving the way for broader practical applications.

6 Conclusions

With the increasing demand for miniaturization and intelligence, integrated polarization detectors have become the primary focus of future polarization detection technologies. The development of these detectors focuses on two main objectives：enhancing polarization detection performance and incorporating new optical dimensional sensing capabilities. Integrated polarization detectors have achieved extinction ratios as high as infinity, while polarization-dependent balanced detectors enable highly sensitive detection of the changes in the polarization state. These advancements allow for the sensing of additional Stokes parameters and even other dimensions of information from the incident light. Despite significant progress，challenges persist in device design principles and fabrication techniques. Moving forward, the adoption of innovative fabrication methods and materials will further elevate detector performance. Additionally, integrating artificial intelligence algorithms is expected to substantially enhance the efficiency and accuracy of

Table 2 Comparison of integrated polarization detectors with innovative features and commercial devices

表2　具有变革性特征的集成式偏振探测器与商用器件的对比

Materials	Gr/Au antenna	Gr/Au antenna	MoS$_2$/Au antenna	MoS$_2$/Au antenna	PAX 1000	ERM 200	DXM 20AF
Responsivity	15. 6 V W^{-1}	27 V W^{-1}	0. 4 mA W^{-1}	0. 5 mA W^{-1}	—	0. 48 A W^{-1}	0. 9 A W^{-1}
Bandwidth	1. 5 MHz	670 GHz	30 kHz	51 kHz	400 Hz	10 Hz	20 GHz
Noise（Hz$^{-1/2}$）	10 nV	2 nV	0. 5 pA	0. 53 pA	—	—	—
NEP（Hz$^{-1/2}$）	0. 64 nW	124 pW	—	1. 7 nW	—	—	28 pW
Dynamic Range（μW）	$10^{-2} \sim 10^2$	0. 07 ~ 3. 06	—	5. 7 ~ 13. 3	$10^{-3} \sim 10^4$	—	<10^4
PER	∞, -1	∞, -1	∞, -1	—	—	10^4	—
Stokes Parameters	S_1	S_1	S_3	S_1, S_2, S_3	S_1, S_2, S_3	S_1, S_2	—
NE$\Delta\chi$,（degree Hz$^{-1/2}$）	0. 02	—	0. 009	—	—	0. 01	—
Ref.	23	35	16	17	Thorlabs	Thorlabs	Thorlabs

multi-Stokes parameter reconstruction and the interpretation of high-dimensional optical information.

Acknowledgment

References

[1] Rubin N A, D'Aversa G, Chevalier P, et al. Matrix Fourier optics enables a compact full-Stokes polarization camera [J]. Science, 2019, 365 (6448): eaax1839.

[2] Zhang L, Zhou C, Liu B, et al. Real-time machine learning-enhanced hyperspectro-polarimetric imaging via an encoding metasurface[J]. Science Advances, 2024, 10(1): eadp5192.

[3] Kuang Y, Wang S, Mo B, et al. Palm vein imaging using a polarization-selective metalens with wide field-of-view and extended depth-of-field[J]. NPJ Nanophotonics, 2024, 1(1): 24.

[4] Zaidi A, Rubin N A, Meretska M L, et al. Metasurface-enabled single-shot and complete Mueller matrix imaging[J]. Nature Photonics, 2024, 18(7): 704-712.

[5] Togan E, Chu Y, Trifonov A S, et al. Quantum entanglement between an optical photon and a solid-state spin qubit [J]. Nature, 2010, 466(7307): 730-734.

[6] Greve K D, Yu L, McMahon P L, et al. Quantum-dot spin-photon entanglement via frequency downconversion to telecom wavelength [J]. Nature 2012, 491(7424), 421-425.

[7] Rosskopf M, Mohr T, Elsäßer W. Ghost polarization communication [J]. Physical Review Applied, 2020, 13(3): 034062

[8] Han Y, Li G. Coherent optical communication using polarization multiple-input-multiple-output [J]. Optics Express, 2005, 13(19): 7527-7534.

[9] VanWiggeren, G D; Roy R. Communication with dynamically fluctuating states of light polarization[J]. Physical review letters, 2002, 88 (9): 097903.

[10] Gaiarin S, Perego A M, da Silva E P, et al. Dual-polarization nonlinear Fourier transform-based optical communication system [J]. Optica, 2018, 5(3): 263.

[11] Liu J, Zhang D, Yu D, et al. Machine learning powered ellipsometry [J]. Light: Science & Applications, 2021, 10(1): 55.

[12] Backer A S, Biebricher A S, King G A, et al. Single-molecule polarization microscopy of DNA intercalators sheds light on the structure of S-DNA[J]. Science Advances, 2019, 5(1): eaav1083.

[13] Dong P, Zong C, Dagher Z, et al. Polarization-sensitive stimulated Raman scattering imaging resolves amphotericin B orientation in Candida membrane[J]. Science Advances, 2021, 7(1): eabd5230.

[14] He C, He H, Chang J, et al. Polarisation optics for biomedical and clinical applications: A review[J]. Light: Science & Applications, 2021, 10(1): 194.

[15] Lu J, Xue Y, Bernardino K, et al. Enhanced optical asymmetry in supramolecular chiroplasmonic assemblies with long-range order[J]. Science, 2021, 371(6536): 1368 - 1374.

[16] Bu Y, Ren X, Zhou J, et al. Configurable circular-polarization-dependent optoelectronic silent state for ultrahigh light ellipticity discrimination[J]. Light: Science & Applications, 2023, 12(1): 176.

[17] Deng J, Shi M, Liu X, et al. An on-chip full-Stokes polarimeter based on optoelectronic polarization eigenvectors [J]. Nature Electronics, 2024, 7(11): 1004-1014.

[18] Li L, Wang J, Kang L, et al. Monolithic full-stokes near-infrared polarimetry with chiral plasmonic metasurface integrated graphene-silicon photodetector [J]. ACS Nano, 2020, 14 (12): 16634 - 16642.

[19] Fang C, Li J, Zhou B, et al. Self-powered filterless on-chip full-stokes polarimeter[J]. Nano Letters, 2021, 21(14): 6156-6162.

[20] Andreou A G; Kalayjian Z K. Polarization imaging: principles and integrated polarimeters [J]. IEEE Sensors Journal, 2002, 2(6): 566-576.

[21] Tyo J S, Goldstein D L, Chenault D B, et al. Review of passive imaging polarimetry for remote sensing applications [J]. Applied optics, 2005, 45(22): 5453-5469.

[22] Zhou J, Deng J, Shi M, et al. Cavity coupled plasmonic resonator enhanced infrared detectors [J]. Applied Physics Letters, 2021, 119 (16): 160504

[23] Wei J, Xu C, Dong B, et al. Mid-infrared semimetal polarization detectors with configurable polarity transition [J]. Nature Photonics, 2021, 15(8): 614-621.

[24] Wei J, Chen Y, Li Y, et al. Geometric filterless photodetectors for mid-infrared spin light [J]. Nature Photonics, 2022, 17 (1): 171-178.

[25] Dai M, Wang C, Qiang B, et al. Long-wave infrared photothermoelectric detectors with ultrahigh polarization sensitivity [J]. Nature Communications, 2023, 14(1): 3421.

[26] Dai X, Yu Y, Ye T, et al. Dynamically reconfigurable on-chip polarimeters based on nanoantenna enabled polarization dependent optoelectronic computing[J]. Nano Letters, 2024, 24(3): 983-992.

[27] Zhao S, Wu J, Jin K, et al. Highly polarized and fast photoresponse of black phosphorus-inse vertical p-n heterojunctions[J]. Advanced Functional Materials, 2018, 28(34): 1802011.

[28] Yu Y, Dai Z, Guan H, et al. Blackbody-sensitive uncooled infrared detector with ultra-broadband and ultrafast photoresponse based on Te/WTe₂ heterostructure[J]. Advanced Optical Materials, 2024, 12 (25): 2400776.

[29] Dai Z, Yu Y, Guan H, et al. Room-temperature blackbody-sensitive photodetector with visible-to-long-wavelength-infrared photoresponse and ultrafast speed based on a Te/PtSe₂ heterostructure [J]. Advanced Electronic Materials, 2024: 2400268.

[30] Bai R, Xiong T, Zhou J, et al. Polarization-sensitive and wide-spectrum photovoltaic detector based on quasi-1D ZrGeTe₄ nanoribbon [J]. InfoMat, 2021, 4(3): e12258.

[31] Ye L, Wang P, Luo W, et al. Highly polarization sensitive infrared photodetector based on black phosphorus-on-WSe₂ photogate vertical heterostructure[J]. Nano Energy, 2017, 37: 53-60.

[32] Castilla S, Vangelidis I, Pusapati V, et al. Plasmonic antenna coupling to hyperbolic phonon-polaritons for sensitive and fast mid-infrared photodetection with graphene [J]. Nature Communications, 2020, 11(1): 4872.

[33] Yuan H, Liu X, Afshinmanesh F, et al. Polarization-sensitive broadband photodetector using a black phosphorus vertical p-n junction[J]. Nature Nanotechnology, 2015, 10(8): 707-713.

[34] Chen Y, Tan T, Wang Z, et al. Momentum-matching and band-alignment van der Waals heterostructures for high-efficiency infrared photodetection[J]. Science Advances, 2022, 8(1): eabq1781.

[35] Wei J, Li Y, Wang L, et al. Zero-bias mid-infrared graphene photodetectors with bulk photoresponse and calibration-free polarization detection[J]. Nature Communications, 2020, 11(1): 6404.

[36] Zhang G, Lyu X, Qin Y, et al. High discrimination ratio, broadband circularly polarized light photodetector using dielectric achiral nanostructures[J]. Light: Science & Applications, 2024, 13(1): 275.

[37] Li D, Li Z, Sun Y, et al. In-sublattice carrier transition enabled polarimetric photodetectors with reconfigurable polarity transition [J]. Advanced Materials, 2024, 36(36): 2407010.

[38] Wang H, Li Y, Gao P, et al. Polarization-and gate-tunable optoelectronic reverse in 2D semimetal/semiconductor photovoltaic heterostructure[J]. Advanced Materials, 2023, 36(6): 2309371.

[39] Wu S, Deng J, Wang X, et al. Polarization photodetectors with configurable polarity transition enabled by programmable ferroelectric-doping patterns[J]. Nature Communications, 2024, 15(1): 8743.

[40] Shen J, Zhu T, Zhou J, et al. High-discrimination circular polarization detection based on dielectric-metal-hybrid chiral metamirror integrated quantum well infrared photodetectors[J]. Sensors, 2022, 23 (1): 168.

[41] Dai M, Wang C, Qiang B, et al. On-chip mid-infrared photothermoelectric detectors for full-Stokes detection [J]. Nature Communications, 2022, 13(1): 4560.

[42] Guo S, Zhang D, Zhou J, et al. Enhanced infrared photoresponse in-

duced by symmetry breaking in a hybrid structure of graphene and plasmonic nanocavities[J]. Carbon, 2020, 170: 49-58.

[43] Zhang D, Zhou J, Liu C, et al. Enhanced polarization sensitivity by plasmonic-cavity in graphene phototransistors[J]. Journal of Applied Physics, 2019, 126(7): 074301

[44] Peng J, Cumming B P, Gu M. Direct detection of photon spin angular momentum by a chiral graphene mid-infrared photodetector[J]. Optics letters, 2019, 44(12): 2998-3001.

[45] Li F, Chu Z, Zhou J, et al. Compact on-chip THz circular polarization detectors with high discrimination based on chiral plasmonic antennas[J]. Optical Materials Express, 2023, 13(11): 3330-3341.

[46] Wu S, Chen Y, Wang X, et al. Ultra-sensitive polarization-resolved black phosphorus homojunction photodetector defined by ferroelectric domains[J]. Nature Communications, 2022, 13(1): 3198.

[47] Xie J, Ren Z, Wei J, et al. Zero-bias long-wave infrared nanoantenna-mediated graphene photodetector for polarimetric and spectroscopic sensing[J]. Advanced Optical Materials, 2023, 11(9): 2202867.

[48] Lu F, Lee J, Jiang A, et al. Thermopile detector of light ellipticity [J]. Nature Communications, 2016, 7(1): 12994.

[49] Thomaschewski M, Yang Y, Wolff C, et al. On-chip detection of optical spin-orbit interactions in plasmonic nanocircuits[J]. Nano Letters, 2019, 19(2): 1166-1171.

[50] Zuo J, Bai J, Choi S, et al. Chip-integrated metasurface full-Stokes polarimetric imaging sensor[J]. Light: Science & Applications, 2023, 12(1): 218.

[51] Arbabi E, Kamali S M, Arbabi A, et al. Full-stokes imaging polarimetry using dielectric metasurfaces[J]. ACS Photonics, 2018, 5

(8): 3132-3140.

[52] Sun C, Sun D, Bo Y, et al. Fabrication and performance analysis of infrared InGaAs polarimetric detector with complete coverage of superpixel-structured grating[J]. Infrared Physics & Technology, 2022, 123: 104066.

[53] Feng B, Shi Z, Liu H, et al. Polarized-pixel performance model for DoFP polarimeter[J]. Journal of Optics, 2018, 20(6): 065703.

[54] Ma J, Fang C, Liang L, et al. Full-stokes polarimeter based on chiral perovskites with chirality and large optical anisotropy[J]. Small, 2021, 17(47): 2103855.

[55] Ma C, Yuan S, Cheung P, et al. Intelligent infrared sensing enabled by tunable moire quantum geometry[J]. Nature, 2022, 604(7905): 266-272.

[56] Jiang H, Chen Y, Guo W, et al. Metasurface-enabled broadband multidimensional photodetectors[J]. Nature Communications, 2024, 15(1): 8347.

[57] Wang F, Zhu S, Chen W, et al. Multidimensional detection enabled by twisted black arsenic–phosphorus homojunctions[J]. Nature nanotechnology, 2024, 19(4): 455-462.

[58] Zhang S, Jiao H, Chen Y, et al. Multi-dimensional optical information acquisition based on a misaligned unipolar barrier photodetector [J]. Nature Communications, 2024, 15(1): 7071.

[59] Fan Q, Xu W, Hu X, et al. Trilobite-inspired neural nanophotonic light-field camera with extreme depth-of-field[J]. Nature Communications, 2022, 13(1): 2130.

[60] Fan Y, Huang W, Zhu F, et al. Dispersion-assisted high-dimensional photodetector[J]. Nature, 2024, 630(8015): 77–83.